Condensation-induced self-patterning of a thin clayey layer

Jérôme Martin, Frédéric Doumenc

Condensation–induced self–patterning of a thin clayey layer

J. Martin[1] and F. Doumenc[1,2]

[1] *Université Paris-Saclay, CNRS, FAST, 91405, Orsay, France*
[2] *Sorbonne Université, UFR 919, 4 Place Jussieu, F-75252, Paris Cedex 05, France*

Abstract – We show through laboratory experiments that the self–patterning of a thin clayey layer can be triggered by condensation. The natural sediment used in the experiments was a highly polydisperse granular paste with smectite clay in the fine fraction. Under certain physicochemical conditions, condensation induces the solid–to–liquid transition of the sediment layer, resulting in sediment flow and the formation of band structures. These results suggest a physical mechanism for the formation of patterns commonly observed on the humid walls of underground cavities, referred to as vermiculations.

Introduction. – It has been well known for more than a century that the sedimentary material lying on the humid walls of underground cavities can self–organize to form a wide variety of patterns, called vermiculations (see for instance Adesso *et al* [1] for illustrative examples). Many attempts have been made to explain the formation of these patterns (see reviews in refs. [2, 3]), but a physical mechanism supported by strong evidence remains to be found. Understanding this natural process is, however, of utmost importance for the conservation of painted caves, where valuable prehistoric paintings can be damaged by vermiculation crises [4–6].

The presence of water on cave walls is a necessary but not sufficient condition to obtain vermiculations [2]. When the sediment is saturated with water, it forms a granular paste that behaves as a yield stress fluid [7]. The yield stress, due to colloidal interactions, depends on the chemical composition of the water film present on the wall, through the pH, the ionic strength, or the nature of the ions in solution [8]. These physicochemical parameters may vary in time and space with the origin of the water (percolation, flooding or condensation) [6], or microbiological activity [9]. We show through laboratory experiments that, under certain conditions, condensation reduces the sediment yield stress to zero, resulting in sediment flow and pattern formation.

Material characterization. – In our experiments, we used natural sediment collected in Maillol Cave (Montignac, France) in a limestone massif. The particle size distribution of this material is highly polydisperse. It spreads from 1 μm to 1 mm, with a significant fraction of fine particles (16% in volume under 10 μm). The mineralogical composition of Maillol Cave sediment was determined by X-ray diffraction. It consists of high quantities of quartz (silica) and calcite (calcium carbonate, $CaCO_3$), with lower amounts of many other minerals such as metallic oxides, hydroxides, and various clay minerals (phyllosilicates) with a predominance of smectites (80% of the fine fraction) [7]. Before use, the sediment was dried in ambient air and then smoothly crushed with a mortar. All particles with a

diameter above 200 μm (4% volume fraction) were removed by dry sieving. A granular paste was finally obtained by mixing the dried powder with a given amount of water previously saturated with $CaCO_3$. The initial volume fraction of solid in the sediment paste was set to 0.440 ± 0.012 for all experiments. The corresponding yield stress was 2300 ± 400 Pa (as a comparison, the gravity–induced shear stress on a vertical 100 μm–thick sediment layer is of the order of 1 Pa).

The rheological behavior of Maillol Cave sediment was recently studied by Freydier *et al* [6, 7]. They showed that the yield stress of this material could go to zero if it was first soaked in an aqueous solution containing a salt with a monovalent cation (e.g., NaCl) and then placed in deionized (DI) water. This solid–to–liquid transition of the sediment was not observed if the aqueous solution used in the first step of the process contained a salt with a multivalent cation (e.g., $CaCl_2$), or if the sediment sample was directly soaked in DI water.

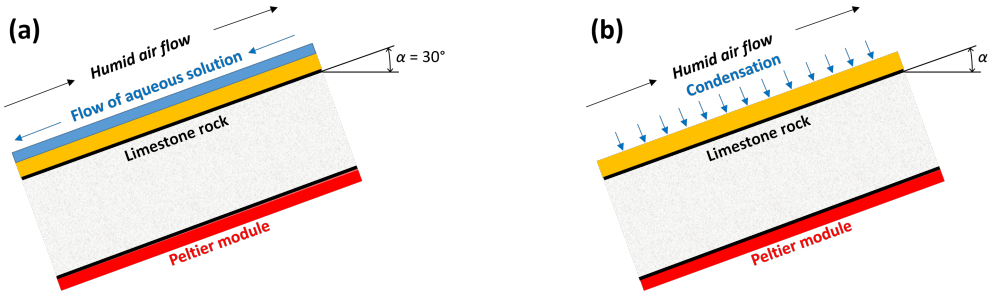

Fig. 1: Experimental protocol. (a) First step: aqueous solution flowing film; (b) Second step: condensation. The sediment layer coated on the rock is shown in yellow.

This striking behavior is characteristic of smectites. Indeed, the faces of smectite platelets carry permanent negative charges. They are balanced by the cations of the diffuse double layers, whose valence strongly affects the smectite phase diagram. In a smectite paste with monovalent counterions (e.g., Na^+), interparticle forces are attractive for salt concentrations greater than the critical coagulation concentration (CCC), typically of the order of 10 mmol/L. In a smectite paste with multivalent counterions (e.g., Ca^{2+}), interparticle forces are always attractive [10–12]. This accounts for the experimental results of Freydier *et al* [6, 7]. During the first soaking in a NaCl solution, Na^+ was substituted for Ca^{2+} in the diffuse double layers, but the sediment yield stress was still significant because the NaCl concentration was greater than the CCC. Interparticle interactions turned to repulsion in the subsequent soaking in DI water, which resulted in the gel–sol transition of smectite, and the collapse of the sediment yield stress. This rheological behavior reveals that particles of various compositions and sizes included in the sediment are bound together by a smectite gel, which is responsible for the material yield stress.

Experimental setup. – An experimental setup was designed to demonstrate that the sediment loss of cohesion could induce self–patterning under cave environmental conditions. It enables the exposure of a sediment thin layer to a flow at specific physicochemical conditions followed by condensation at a controlled rate (see fig. 1 for a sketch of the setup, and the Supplementary Material for more details).

A thin layer of sediment paste was coated on the rectangular surface of the limestone rock (80×55 mm). The same rock sample was used for all experiments (after each experiment, the rock was cleaned with tap water and rinsed with DI water previously saturated with $CaCO_3$). The coating was done using a film applicator with a 200 μm–gap (Elcometer, ref. 3540). However, because of the waviness of the rock surface (measured with a comparator), the actual local gap between the rock surface and the applicator could vary from 100 to 200 μm. We can thus assume that the mean thickness of the sediment layer was approximately 150 μm

with spatial fluctuations lower than 50 μm. The reproducibility of the deposit thickness was tested by weighing the rock before and after coating. The mass measurement of 7 deposits yielded a mean thickness of 163 μm and a standard deviation of 15 μm.

The coated stone was then inserted in a thermostatically controlled enclosure at 15.05°C, which could be tilted at an angle α from the horizontal position ($0 \leq \alpha \leq 85°$). This enclosure was closed with transparent double glazing to allow observation of the sediment layer. Humid air precooled at the enclosure temperature (15.05°C) permanently flowed above the sediment layer with a mass flow rate of 0.215 g/s, CO_2 partial pressure (pCO_2) of 35 Pa and a dew point of 14.92°C. Two temperature sensors were inserted into the limestone rock, which rested on two Peltier modules (small heat pumps in the form of 40×40 mm square plates). The rock thickness was 20 mm and the temperature sensors were located 9 mm below the upper surface of the rock. This device allowed us to control the rock temperature independently of its surroundings.

In the first step of each experiment, the rock temperature was set to 15.00°C to prevent condensation. The tilt angle α was set to 30°. An aqueous solution containing 20 mmol/L of NaCl and saturated with $CaCO_3$ at the same pCO_2 as the air flow ($[Ca^{2+}] \simeq 0.6$ mmol/L, pH $\simeq 8.2$, ionic strength $\simeq 22$ mmol/L) was injected with a syringe pump at the top of the setup at a constant flow rate of 100 mL/h. The solution flowed above the sediment layer by gravity drainage (fig. 1a). From lubrication theory, we estimate that the height of the liquid film was approximately a few tens of microns, resulting in a viscous stress on the sediment layer of less than 1 Pa. Note that the solution had been previously saturated with $CaCO_3$ to avoid the dissolution of sediment calcite during this step. After 3 hours, the syringe pump providing the flow of the aqueous solution was stopped.

In the second step, immediately after stopping the syringe pump, the set-point of the rock temperature was decreased below the dew point of the air to trigger water condensation at the surface of the sediment layer. After a transient regime due to the thermal inertia of the rock, the condensation rate was expected to be proportional to ΔT, the temperature drop between the air dew point and the rock temperature (see fig. 1b). The time τ_{th} required to achieve 90% of the temperature drop was systematically measured in all experiments. τ_{th} globally increased with ΔT, in the range from 2 min to 17 min. Assuming 8×10^{-7} m^2/s for the limestone diffusivity, the thermal diffusion time between the temperature sensors and the sediment layer was approximately 2 min. The temperature sensors and the rock upper surface thus reached the steady state approximately at the same time. We also determined the time for the drainage of the liquid film after stopping the syringe pump. The sediment layer was illuminated with a laser sheet. After stopping the syringe pump, the image of the laser sheet reflected on a white screen showed that the transition from specular reflection (presence of a liquid film) to diffuse reflection (due to sediment roughness) was achieved within a time of approximately 3 min. This drainage time does not exceed τ_{th}, the duration of the thermal regime. τ_{th} is thus used to estimate the uncertainty on the initial time. If modified, the tilt angle α was changed after a waiting time of 10 min to allow prior drainage of the aqueous solution.

To characterize the setup, the coated rock was weighed before and after being exposed to condensation at a given ΔT, before self–patterning began. These experiments provided the absorption rate q, defined as the volumetric flow rate of condensed water absorbed by a unit surface of sediment layer. We checked that no liquid flowed out from the rock during the condensation stage prior to pattern formation (we only noticed a few droplets under the rock after the end of the experiments performed at the highest temperature drop, i.e., $\Delta T \simeq 11$ K). The absorption rate q is thus expected to approximately equal the condensation rate, which accounts for the scaling $q \propto \Delta T$ observed in fig. 5a.

Results. – Figure 2 displays the initial state and the final pattern for $\alpha = 85°$ and $\Delta T = 3.3$ K. Video 1 in the Supplementary Material shows the same experiment. The origin of time is taken at the beginning of the second step (i.e., when the set–point of the

rock temperature was decreased). No modification of the sediment layer is observed during the first step, i.e, during the flow of the NaCl–$CaCO_3$ solution (this remark applies to all experiments presented in this paper). Self–patterning takes place during the second step. Sediment motion begins approximately at times $t_1 \simeq 128\,\text{min}$ and $t_2 \simeq 188\,\text{min}$ at 2 cm from bottom and top edges, respectively. For all experiments, we define the onset time as $t_{sp} = (t_1 + t_2)/2$. In the specific case of fig. 2, $t_{sp} \simeq 158\,\text{min}$. The whole surface is covered with band structures at time $t \simeq 270\,\text{min}$, and no significant motion is observed after $t \simeq 290\,\text{min}$.

We see in fig. 3 that the same kind of pattern develops for a smaller tilt angle ($\alpha = 30°$) and a wide range of temperature drops, from $\Delta T \simeq 0.3\,\text{K}$ to $\Delta T \simeq 11\,\text{K}$ (movie 2 in the Supplementary Material shows the full patterning process for the case $\Delta T = 3.3\,\text{K}$). This highlights the robustness of the underlying mechanism leading to the accumulation of particles in the band structures. Increasing ΔT enhances the contrast of the final pattern, with no obvious effect on its morphology.

Fig. 2: (a) Initial state and (b) final pattern for $\alpha = 85°$ and $\Delta T = 3.3\,\text{K}$ (image size: $80 \times 55\,\text{mm}$).

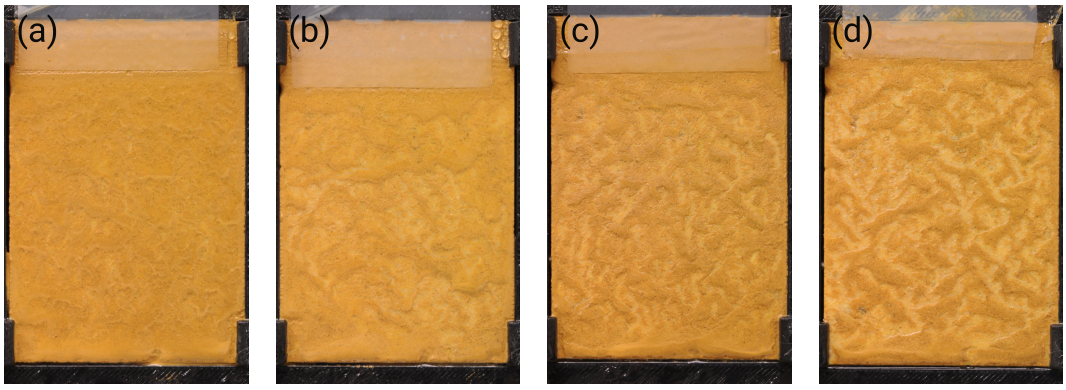

Fig. 3: Effect of the temperature drop ΔT on the final pattern for $\alpha = 30°$. (a) $\Delta T = 0.31\,\text{K}$; (b) $\Delta T = 1.1\,\text{K}$; (c) $\Delta T = 3.3\,\text{K}$; (d) $\Delta T = 11.0\,\text{K}$ (image size: $80 \times 55\,\text{mm}$).

Discussion. – Cation substitutions are a prerequisite for condensation–induced self–patterning. This was easily demonstrated by removing the NaCl from the aqueous solution running on the sediment layer during the first step of the experiment. When a $CaCO_3$–saturated and NaCl–free solution was used, no sediment motion was observed after 24 hours of condensation at $\Delta T \simeq 11\,\text{K}$ (see the final state of the sediment layer in fig. 4a). With the NaCl–$CaCO_3$ solution during the first step, Na^+ ions are substituted for Ca^{2+} in the smectite

Fig. 4: Final states with no pattern: (a) $\alpha = 30°$, $\Delta T = 11.1\,\mathrm{K}$, $CaCO_3$ solution during first step; (b) $\alpha = 0°$, $\Delta T = 3.1\,\mathrm{K}$, NaCl–$CaCO_3$ solution during first step. Condensation for 24 hours in both cases (image size: $80 \times 55\,\mathrm{mm}$).

diffuse double layers. Ca–smectite, which is always in a gel state, becomes a Na–smectite, which is expected to disperse at low enough ionic strength. As no motion is observed in the sediment layer, one infers that the ionic strength of the aqueous solution is high enough to maintain the Na–smectite in a gel state. This is consistent with the rheological measurements displayed in table 1. After a 24 hours long soaking in the NaCl–$CaCO_3$ solution (same as the one injected in the first step), the sediment yield stress decreased by an order of magnitude but was still of the order of a few hundreds of Pascals, considerably above the stresses induced by gravity and by the flow of the aqueous solution ($\sim 1\,\mathrm{Pa}$).

We turn now to the second step of the experiment. When the injection of the solution is stopped, the liquid film above the sediment layer is drained away by gravity, but the sediment pores are still filled with the injected NaCl–$CaCO_3$ solution. In the following condensation step, however, the pore liquid is diluted by the intake of condensed water. This causes a decrease of the ionic strength resulting in the gel–sol transition of the smectites, the collapse of the sediment yield stress, and finally the flow of the sediment layer due to gravity (no motion is observed for $\alpha = 0$, which proves the role of gravity, see fig. 4b). At this point, the sediment behaves as a suspension of macroscopic particles. Indeed, particles greater than $10\,\mu\mathrm{m}$ represent 84% of the particle size distribution, and these particles are no longer bound by the smectite gel. Hence, the mechanism proposed by Buchanan *et al* [13] to describe the formation of band structures for noninteracting particles is likely to apply. When the sediment flows, its thickness decreases. Due to the confinement by the free surface, some isolated particles are pinned by solid friction with the substrate. The subsequent accumulation of particles in band structures results from the jamming induced by convergent streamlines around the pinned particle and by further accumulation of particles in the jammed region acting as a filter [14].

Table 1: solid volume fraction φ_s and yield stress τ_c of sediment samples in the initial state and after a 24 hours long soaking in an aqueous solution of 20 mmol/L NaCl saturated with $CaCO_3$ (1–mm thick sample containing $2\,\mathrm{cm}^3$ of sediment soaked in 250 mL of solution, see ref. [6] for a detailed description of the rheological measurements).

	φ_s	τ_c / Pa
Initial state	0.440 ± 0.001	2300 ± 200
After soaking	0.389 ± 0.004	330 ± 70

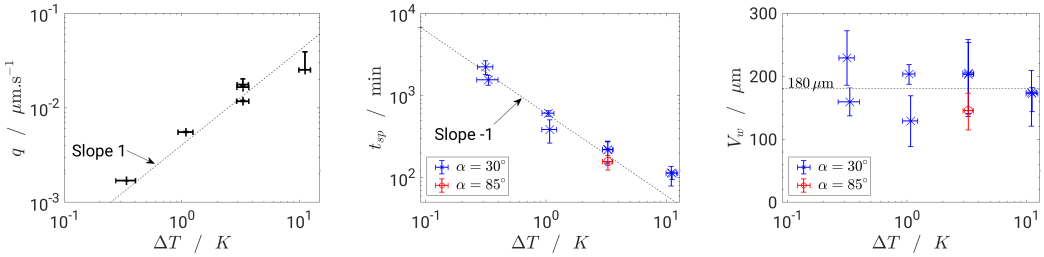

Fig. 5: Effect of the temperature drop ΔT on (a) the absorption rate q; (b) the onset time t_{sp}; (c) The corresponding volume of condensed water per unit of surface $V_w = q\,t_{sp}$. The error bars on ΔT show the difference between the temperatures measured by both sensors located in the rock. The error bars on q stem from the uncertainties on the measurement of the mass variation of the sediment layer due to condensation and the time during which it was exposed to condensation. The upper and lower error bars on t_{sp} are $|t_1 - t_2|/2$ and $(\tau_{th} + |t_1 - t_2|/2)$, respectively. The uncertainty on V_w is derived from the uncertainties on q and t_{sp}.

In the following, we investigate in more detail the onset of the self–patterning process triggered by the solid–to–liquid transition of the sediment layer, prior to which it cannot flow. Let $V_w = q\,t_{sp}$ be the volume of condensed water per unit of surface at the onset of self–patterning. It results from the scalings $q \propto \Delta T$ (fig. 5a) and $t_{sp} \propto \Delta T^{-1}$ (fig. 5b) that V_w is almost constant (fig. 5c). Averaging all of the experimental results yields $V_w \simeq 180 \pm 60\,\mu$m. It is worth noticing that this constant value of V_w was obtained for onset times t_{sp} varying over a decade (from 100 min to 2000 min, see fig. 5b), suggesting negligible kinetic effects over the experiment time scales.

It is possible to ascertain that the constant value of V_w is consistent with the rheological behavior of the sediment. As the onset of self–patterning is reached at a fixed dilution factor of the pore solution, the concentration $[\mathrm{NaCl}]_{sp}$ at the onset is constant and it is given by the relation

$$[\mathrm{NaCl}]_{sp} \simeq [\mathrm{NaCl}]\,\frac{h\,(1-\varphi_s)}{h\,(1-\varphi_s)+V_w}\,, \tag{1}$$

where the NaCl concentration [NaCl], the deposit height h and the solid volume fraction φ_s should be assessed at the end of step 1. However, the sediment swelling during step 1 can be neglected (table 1 shows that the solid volume fraction decreased by only 0.051 after 24 hours soaking), so that h and φ_s can be approximated by their initial values. With $[\mathrm{NaCl}] \simeq 20$ mmol/L, $h \simeq 150\,\mu$m and $\varphi_s \simeq 0.44$, eq. (1) yields $[\mathrm{NaCl}]_{sp} \simeq 6$ mmol/L. As NaCl corresponds to the dominant species in the solution, $[\mathrm{NaCl}]_{sp}$ is an estimation of the ionic strength at the onset. Its constant value is therefore in accordance with a corresponding gel–sol transition of the Na–smectites. This interpretation has been tested with the help of rheological characterization of sediment samples successively soaked in two NaCl aqueous solutions saturated with $CaCO_3$. The first soaking was 24 h long in a bath at a fixed concentration [NaCl] = 20 mmol/L (same condition as in table 1), whereas the second soaking was shorter (3 h ± 30 min, chosen for experimental convenience) at bath concentrations varied from 0 to 20 mmol/L. We see in fig. 6 that the yield stress after these two soakings collapses from approximately 300 Pa to 0 when the NaCl concentration of the second soaking is decreased from 10 mmol/L to a value ranging from 3 to 2 mmol/L. The agreement with the value $[\mathrm{NaCl}]_{sp} \simeq 6$ mmol/L predicted by eq. (1) is quite satisfying if we consider that both configurations, condensation and soaking, are quite different (e.g., there is ion exchanges across the sample surface in soaking experiments, not during condensation). This result confirms that the self–patterning onset is controlled by the yield stress collapse due to the gel–sol transition of the Na-smectite gel.

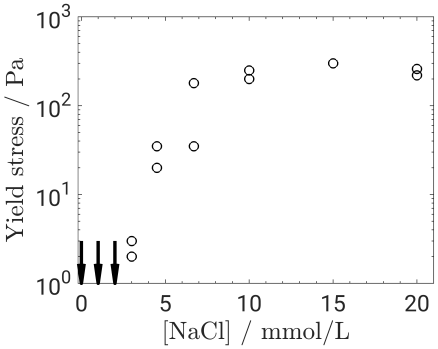

Fig. 6: sediment yield stress τ_c after two successive soakings in NaCl solutions saturated with $CaCO_3$. NaCl concentration of the first soaking was fixed to 20 mmol/L. τ_c is plotted as a function of the NaCl concentration of the second bath. Black arrows correspond to concentrations for which no yield stress was detected (1–mm thick sample containing 2 cm^3 of sediment soaked in 250 mL of solution, see ref. [6] for a detailed description of the rheological measurements).

Conclusion. – These laboratory experiments demonstrate that the self–patterning of a clayey layer can be triggered by water condensation. Transposed to the natural cave environment, our experimental two–step process might correspond to a first time period in which the concentration in monovalent cations increases (due, for instance, to evaporation or microbiological activity), followed by a condensation event during a second time period. Other scenarios are also possible, since the rheology of smectites can be strongly modified by the pH [15], or the presence of multivalent anions [16–18]. In general, any change in the physicochemical conditions leading to the solid–to–liquid transition of a granular paste layer should result in the formation of new patterns or the evolution of existing patterns.

* * *

The experimental setup used in this study was built in the framework of the project "Vermiculations in Lascaux Cave" funded by the French Ministry of Culture (Direction des Affaires Culturelles de Nouvelle-Aquitaine). We thank P.-Y. Jeannin from SISKA for sharing his knowledge about karst systems through many useful discussions. We gratefully thank A. Aubertin, L. Auffray, J. Amarni, R. Pidoux, and C. Manquest (FAST Laboratory) for technical support. We thank D. Calmels, C. Quantin, G. Monvoisin, O. Dufaure, and S. Miska (GEOPS Laboratory) for chemical analysis and geological characterization of our samples and M. Rossi (IJLRA) for useful discussions.

REFERENCES

[1] Addesso R., Bellino A., D'Angeli I. M., De Waele J., Miller A. Z., Carbone C. and Baldantoni D., *Catena*, **182** (2019) 104178.
[2] Bini A., Cavalli Gori M. and Gori S., *Int. J. Speleol.*, **10** (1978) 11.
[3] Hœrlé S., *Reports on "Vermiculations in Lascaux cave", French Ministry of Culture,* unpublished (2012).
[4] Clottes J., *Gallia Préhistoire*, **24** (1981) 525.
[5] Hœrlé S., Konik S. and Chalmin É., *Karstologia*, **58** (2011) 29.
[6] Freydier P., Weber E., Martin J., Jeannin P.-Y., Guerrier B. and Doumenc F., *Int. J. Speleol.*, **50** (2021) 289.
[7] Freydier P., Martin J., Guerrier B., Jeannin P.-Y. and Doumenc F., *Rheol. Acta*, **58** (2019) 675.

[8] Larson R. G., *The structure and rheology of complex fluids* (Oxford University Press) 1999.
[9] Barton H.-A. and Northup D.-E., *Journal of Cave and Karst Studies*, **69** (2007) 163 .
[10] Secor R. and Radke C., *Journal of Colloid and Interface Science*, **103** (1985) 237 .
[11] Abend S. and Lagaly G., *Applied Clay Science*, **16** (2000) 201 .
[12] Hedström M., Hansen E.-E. and Nilsson U., Tech. Rep. SKB TR-15-07 (2016).
[13] Buchanan M., Molenaar D., de Villiers S. and Evans R. M. L., *Langmuir*, **23** (2007) 3732.
[14] Haw M. D., *Phys. Rev. Lett.*, **92** (2004) 185506.
[15] Laribi S., Fleureau J., Grossiord J. and Kbir-Ariguib N., *Clays and clay minerals*, **54** (2006) 29.
[16] Lagaly G. and Permien T., *Applied Clay Science*, **9** (1994) 251.
[17] Martin C., Pignon F., Piau J.-M., Magnin A., Lindner P. and Cabane B., *Phys. Rev. E*, **66** (2002) 021401.
[18] Birgersson M., Börgesson L., Hedström M., Karnland O. and Nilsson U., Tech. Rep. SKB TR-09-34 (2009).